Journal of Nuclear Materials 390–391 (2009) 395–397

Contents lists available at ScienceDirect

Journal of Nuclear Materials

journal homepage: www.elsevier.com/locate/jnucmat

Experimental investigations of turbulent structure propagation across a $E \times B$-velocity shear

T. Windisch *, O. Grulke, T. Klinger

MPI for Plasma Physics, EURATOM Association, Wendelsteinstrasse 1, D-17491 Greifswald, Germany

ARTICLE INFO

PACS:
52.25.Fi
52.25.Xz
52.30.Ex
52.35.Kt
52.35.Ra

ABSTRACT

The influence of an externally generated $E \times B$ shear flow on the propagation of structures in drift-wave turbulence is investigated in a linear laboratory plasma device. Spatiotemporal studies of the dynamics of turbulent structures reveal that structures have a radial component of propagation, thereby contributing mainly to the fluctuation induced particle flux and leading to intermittent density fluctuations in the edge plasma. A radially localized radial $E \times B$-velocity shear layer is generated by a biased emissive filament. The shear layer modifies the phase between density and potential fluctuations, which results in a reduction of transport driven by electrostatic turbulence. A shear decorrelation of the structures, i.e. a decrease of their radial correlation length, is not observed.

1. Introduction

Regardless of the specific magnetic field topology, edge turbulence in magnetically confined plasmas is characterized by intermittent fluctuations of the density and potential [1,2]. In recent years it has been shown that intermittent transport events in the scrape-off layer (SOL) are caused by radially propagating turbulent structures [3–5]. The radial propagation is due to convection in the self-consistent potential, which arises from interchange dynamics due to magnetic field curvature [6,7]. Typical radial structure velocities are 10% of the local ion sound speed. The fluctuation induced flux affects several key reactor issues, e.g., heat and particle fluxes to the first wall, recycling, the divertor concept and strongly determines the radial evolution of the plasma profiles. However, radially propagating structures have also been observed in laboratory devices with linear magnetic field geometry without magnetic field curvature [8–10]. In this paper we present investigations of the propagation of turbulent density structures in the linear high-density helicon device VINETA. The governing instability is the drift-wave instability [11]. In weakly developed drift-wave turbulence turbulent structures peel off of a quasi-coherent $m = 1$ drift-wave mode and propagate from the maximum density gradient radially outwards with a velocity of 5–10% of the local ion sound speed [10]. The influence of an externally generated radial velocity shear on the fluctuation dynamics in the plasma edge is investigated. Special attention is paid to the controlled generation on an $E \times B$ shear layer and the changes of the structure dynamics in response to the velocity shear. The paper is organized as follows: Section 2 outlines the experimental setup and diagnostic techniques. In Section 3 the main experimental findings are presented before the results are summarized in Section 4.

2. Experimental setup

The experiments were performed in the linearly magnetized VINETA device [12]. The cylindrical stainless steel vacuum vessel ($L = 4.5$ m, $d = 0.4$ m) is immersed in a set of 36 magnetic field coils, which generate a homogeneous magnetic field of $B \leqslant 0.1$ T. Plasma is produced by a conventional helicon source [13]. The present investigations are done in an Argon plasma with a neutral gas pressure of $p = 0.08$ Pa, a magnetic field of $B = 60$ mT, and a *rf*-power of $P_{rf} = 2.5$ kW. Time-averaged plasma parameters and fluctuations are measured using Langmuir probes. In order to produce a radially sheared azimuthal velocity an electron emissive filament is utilized [14–16]. It consists of a heated tungsten wire (0.5 mm diameter), which covers 1/4 of the circumference at the radial position $r \approx 70$ mm. The heating current is $I = 21$ A and the filament is biased negatively with respect to the local plasma potential. Two bias voltages have been applied: In the following a bias voltage of $U_b = -5$ V is denoted as case B, while a bias voltage of $U_b = -10$ V is denoted as case C. The unperturbed case without electron emission and bias voltage is named case A. Time-averaged plasma parameters profiles without biased filament are shown in Fig. 1(a)–(c) (blue lines).[1] The density profile has a nearly Gaussian shape. Its width is mainly determined by the antenna geometry

* Corresponding author.
E-mail address: tcw@ipp.mpg.de (T. Windisch).

[1] For interpretation to color in Fig. 1, the reader is referred to the web version of this article.

0022-3115/$ - see front matter © 2009 Elsevier B.V. All rights reserved.
doi:10.1016/j.jnucmat.2009.01.093

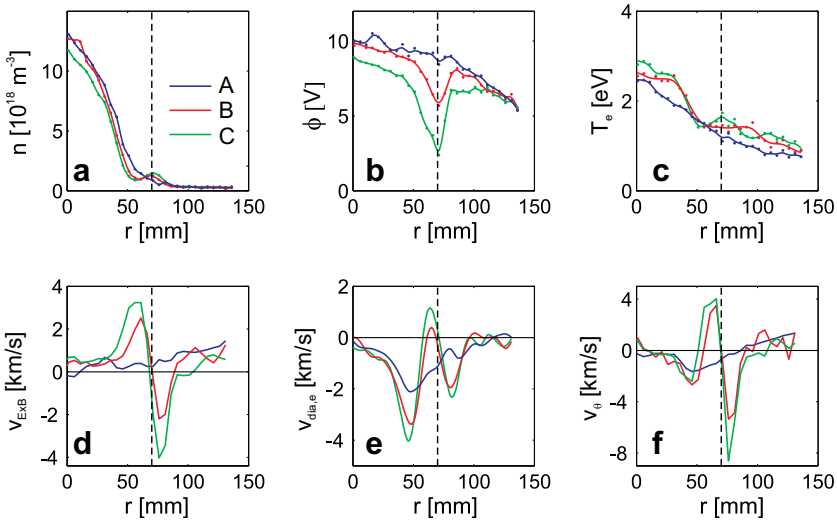

Fig. 1. Time-averaged profiles of plasma density (a), plasma potential (b), electron temperature (c) and corresponding $E \times B$-drift (d), electron diamagnetic drift (e) and the resulting azimuthal drift velocity (f) for the cases A–C (see text for details). The radial position of the filament ($r \approx 70$ mm) is indicated by the dashed line.

(0.1 m diameter). The plasma potential (Fig. 1b) and electron temperature (Fig. 1c) are also peaked in the plasma center and decrease monotonically to the plasma edge. The azimuthal drift velocity $v_\theta = v_{E\times B} + v_{\mathrm{dia,e}}$, is determined by the electron diamagnetic drift $v_{\mathrm{dia,e}} \sim \nabla_r \ln n/B$ and the $E \times B$-drift $v_{E\times B} \sim \nabla_r \phi/B$. The drift velocities are shown Fig. 1(d)–(f). Due to the shape of the time-averaged profiles both drift velocities have opposite directions. In the plasma center $(r < 70\ \mathrm{mm})\, v_{\mathrm{dia,e}}$ dominates over $v_{E\times B}$. In the plasma edge $(r > 75\ \mathrm{mm})\, v_\theta$ is governed by the $E \times B$-velocity. For cases B and C the plasma potential (Fig. 1b) develops a valley at the position of the filament. The depth of the valley increases with negative bias voltage. A direct measurement of the plasma potential profile using a laser heated emissive probe [17] revealed that an influence of non-thermalized electrons is not observed. In general the density profile has the same shape as in the unperturbed case. But at $r = 50$ mm a slight decrease of the density is observed followed by a density hump at $r = 75$ mm. This is mainly caused by the filament geometry. Since the filament does not produce an potential perturbation with azimuthal modenumber $m = 0$ it acts as a large convective cell with closed E × B streamlines, which transports plasma from the density gradient into the plasma edge. As a result of the potential valley the azimuthal velocity v_θ is modified (Fig. 1d–f). In the maximum density gradient $(r \leqslant 50\ \mathrm{mm})\, v_{\mathrm{dia,e}}$ still dominates but for larger radii a radial velocity shear with a maximum shearing rate $\omega \sim \mathrm{rd}/\mathrm{d}r(v_{E\times B}/r)$ of $2 \times 10^4\ \mathrm{s}^{-1}$ in the unperturbed case is found, which increases considerably in cases B and C with $\omega = 4 \times 10^5\ \mathrm{s}^{-1}$ and $\omega = 5.5 \times 10^5\ \mathrm{s}^{-1}$, respectively.

3. Characteristics of fluctuations

The temporal evolution of fluctuations of density $\tilde{n}$, potential $\tilde{\phi}$ and perpendicular particle flux $\tilde{\Gamma} = \tilde{n}\tilde{v}_r$ for situations A and B are depicted in Fig. 2. The corresponding probability distribution function (PDF) are shown as insets. The data is obtained at a radial position $r = 65$ mm close to the inner shear layer edge, axially separated by $z = 1.2$ m from the position of the time-averaged measurements. In both cases the density fluctuations (Fig. 2a and b) show quasi-periodic density bursts with amplitudes $\leqslant 4\sigma$, where σ denotes the standard deviation. The frequency of the bursts is $f \approx 0.5$–1 kHz in case A and becomes more peaked at $f \approx 1$ kHz in case B. The rms-value of the density fluctuations does not change significantly but in case B the PDF becomes more symmetric. The moments of the PDF, i.e. skewness S and kurtosis K, de-

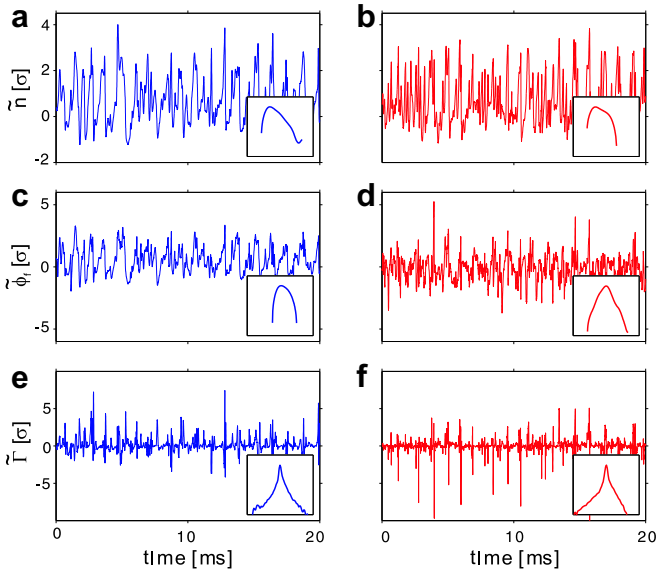

Fig. 2. Time-series of density fluctuations $\tilde{n}$ (a), potential fluctuations $\tilde{\phi}$ (c) and the fluctuating perpendicular particle flux $\tilde{\Gamma}$ (e) close to the inner shear layer ($r = 65$ mm) for case A. The same is shown for case B (b, d, f).

crease significantly from case A ($S = 0.9$, $K = 1.1$) to case B ($S = 0.5$ and $K = -0.2$). In contrast to the density fluctuations the rms-level of potential fluctuations (Fig. 2c and d) in case B is a factor of 1.7 smaller than in the unperturbed case. Here, skewness and kurtosis change from $S = 0.35$ and $K = -0.2$ in case A to $S = 0.1$ and $K = 1.3$ in case B. The fluctuation induced particle flux $\tilde{\Gamma}$ (Fig. 2e and f) exhibits in both cases transport events with high amplitudes. Here, positive events correspond to a flux directed radially outwards. In contrast to the unperturbed case, in which the positive transport events dominate, negative transport events with large amplitudes are observed in case B [9].

As a result the mean particle flux $\langle\tilde{\Gamma}\rangle$ decreases by a factor of 1.3. The transport reduction is not only determined by the decreasing amplitudes of the potential fluctuations but also by the phase $\delta = \measuredangle(\tilde{n}, \tilde{\phi})$, which changes sign from $\delta = 0.05\pi$ in case A to $\delta = -0.2\pi$ in case B at the frequency of the large density events.

The radial evolution of the measured azimuthal phase velocity v_{ph} of density fluctuations across the entire plasma density profile is shown in Fig. 3 for all three cases. The phase velocity is estimated

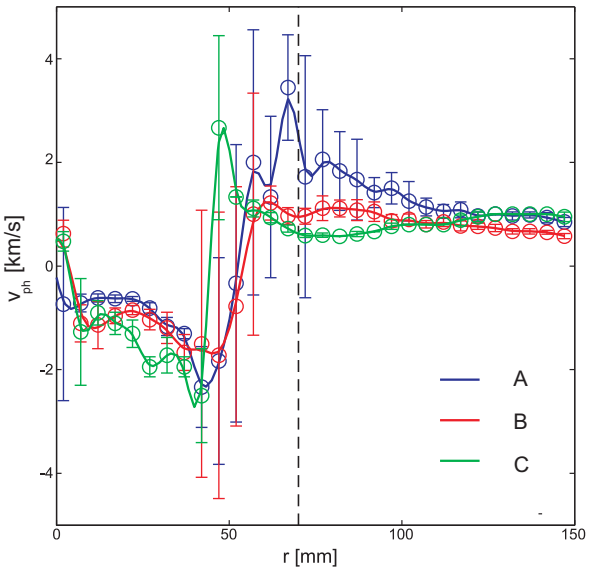

Fig. 3. Radial evolution of the measured azimuthal phase velocity of density fluctuations for cases A–C. The radial position of the filament ($r \approx 70$ mm) is indicated by the dashed line.

using two probes, which are separated azimuthally by 8 mm. The time lag of the cross correlation function (ccf) then yields the phase velocity (averaged in frequency space). In the maximum density gradient region $r = 40$—50 mm v_{ph} is dominated for all cases by the electron diamagnetic drift, which is a result of the governing drift-wave instability. The measured value of $v_{ph} \approx 2$ km/s agrees well with the estimates shown in Fig. 1(f). In the unperturbed case the evolution of v_{ph} is mainly determined by the $E \times B$-drift for larger radii ($r > 70$ mm, cf. Fig. 1d). The electron diamagnetic drift does not contribute since the turbulent structures are disconnected from the quasi-coherent drift modes in the maximum density gradient region [10]. In the outer shear layer region at $r \approx 70$—90 mm the phase velocity decreases from $v_{ph} \approx 2$ km/s in the unperturbed case to $v_{ph} \approx 1$ km/s in case B and to $v_{ph} \approx 0.5$ km/s in case C, which is in qualitative agreement with the results shown in Fig. 1(f). Deviations between the results shown in Figs. 1(f) and 3 are most likely a result of the axial separation of the measurements.

The result of a transport reduction inside the shear layer suggests that the radially propagating turbulent structures, which are the main contributors to $\tilde{\Gamma}$, are strongly affected by the velocity shear. A direct measurement of the transport in the maximum shear layer is rather difficult since the fast electrons emitted from the filaments lead to perturbations of the floating potential fluctuations. In order to investigate this subject spatiotemporal measurements were done. Density fluctuations are recorded simultaneously with a fixed reference probe located outside the shear layer in the plasma edge ($r = 85$ mm) and with a second probe, which is consecutively moved across the entire plasma cross-section. A cross-correlation analysis between the probe signals then yields the spatiotemporal dynamics. The resulting cross-correlation function at time lag $\tau = 0$ is shown in Fig. 4 for cases A and B. At the reference position the shearing rate ω increases from $\omega = 1 \times 10^4$ s^{-1} in case A to $\omega = 2 \times 10^5$ s^{-1} in case B. The shear only affects the turbulent fluctuations if the shear rate is larger than the inverse of the e-folding time τ_e of the auto-correlation function [18]. At the position of the reference probe this yields $1/\tau_e = 6.7 \times 10^3$ s^{-1} for the density fluctuations, which is much smaller than the shear rate if the filament is heated. Comparing the radial correlation lengths in both cases no significant reduction is observed. The decrease of the azimuthal phase velocity at the reference position (cf. Fig. 3) leads to a decreasing azimuthal correlation length.

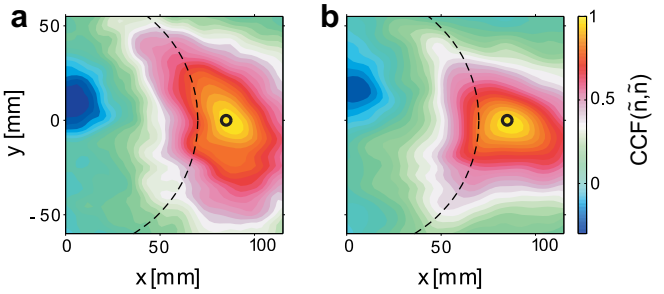

Fig. 4. Two-dimensional cross-correlation function for the cases A (a) and B (b) at time lag $\tau = 0$. The position of the reference probe is outside the shear layer ($r = 85$ mm, indicated by the black circle). The position of the filament is indicated by the dashed line.

4. Summary

It has been demonstrated that an emissive filament is well suited to produce a sheared $E \times B$-flow. The shear layer is localized to the position of the filament. Compared to the situation without filament a reduction of the radial outward particle flux at the inner edge of the shear layer is observed, which is caused by a decrease of the potential fluctuation amplitude and by a change in sign of the phase between density and potential fluctuations. The results of the two-dimensional cross-correlation analysis shows that the radial correlation length of the radially propagating turbulent structures in the plasma edge is not affected by the shear layer. A transport reduction due to the shear decorrelation paradigm [19] is not observed. The measured phase velocity of the fluctuations corresponds to the estimated azimuthal fluid drift velocities although a direct comparison is rather difficult because of uncertainties in the parallel evolution of the shear layer along the magnetic field.

References

[1] V. Carbone, G. Regnoli, E. Martines, V. Antoni, Phys. Plasmas 7 (2000) 445.
[2] J.A. Boedo, D. Rudakov, R. Moyer, S. Krasheninnikov, D. Whyte, G. McKee, G. Tynan, M. Schaffer, P. Stangeby, P. West, et al., Phys. Plasmas 8 (2001) 4826.
[3] J.L. Terry, S.J. Zweben, K. Hallatschek, B. LaBombard, R.J. Maqueda, B. Bai, C.J. Boswell, M. Greenwald, D. Kopon, W.M. Nevins, et al., Phys. Plasmas 10 (2003) 1739.
[4] S.J. Zweben, R.J. Maqueda, D.P. Stotler, A. Keese, J. Boedo, C.E. Bush, S.M. Kaye, B. LeBlanc, J.L. Lowrance, V.J. Mastrocola, et al., Nucl. Fusion 44 (2004) 134.
[5] O. Grulke, J.L. Terry, B. LaBombard, S.J. Zweben, Phys. Plasmas 13 (2006) 012306.
[6] S.I. Krasheninnikov, Phys. Lett. A 283 (2001) 368.
[7] O.E. Garcia, V. Naulin, A.H. Nielsen, J.J. Rasmussen, Phys. Rev. Lett. 92 (2004) 165003.
[8] G.Y. Antar, Phys. Plasmas 10 (2003) 3629.
[9] T.A. Carter, Phys. Plasmas 13 (2006) 010701.
[10] T. Windisch, O. Grulke, T. Klinger, Phys. Plasmas 13 (2006).
[11] C. Schröder, O. Grulke, T. Klinger, V. Naulin, Phys. Plasmas 11 (2004) 4249.
[12] C.M. Franck, O. Grulke, T. Klinger, Phys. Plasmas 9 (2002) 3254.
[13] R.W. Boswell, Plasma Phys. Control. Fus. 26 (1984) 1147.
[14] R.J. Taylor, M.L. Brown, B.D. Fried, H. Grote, J.R. Liberati, G.J. Morales, P. Pribyl, D. Darrow, M. Ono, Phys. Rev. Lett. 63 (1989) 2365.
[15] C. Silva, I. Nedzelskiy, H. Figueiredo, R. Galvao, J. Cabral, C. Varandas, Nucl. Fusion 44 (2004) 799.
[16] C. Silva, H. Figueiredo, I. Nedzelskiy, B. Goncalves, C.A.F. Varandas, Plasma Phys. Control. Fus. 48 (2006) 727.
[17] R. Schrittwieser, C. Ionita, P. Balan, R. Gstrein, O. Grulke, T. Windisch, C. Brandt, T. Klinger, R. Madani, G. Amarandei, et al., Rev. Sci. Instrum. 79 (2008) 083508.
[18] C. Ritz, H. Lin, T. Rhodes, A. Wootton, Phys. Rev. Lett. 65 (1990) 2543.
[19] P. Diamond, S. Itoh, K. Itoh, T. Hahm, Plasma Phys. Control. Fus. 47 (2005) R35.